Hindawi
International Journal of Aerospace Engineering
Volume 2022, Article ID 3071244, 12 pages
https://doi.org/10.1155/2022/3071244

Research Article

Variable Structure Control and Its Ground Experimental Test for the Space Station Robot

Feilong Zhang,[1,2,3] Bi Zhang,[1,2] Bing Han,[4] Danyang Qu,[1,2,3] and Xingang Zhao[1,2]

[1]*State Key Laboratory of Robotics, Shenyang Institute of Automation, Chinese Academy of Sciences, Shenyang 110016, China*
[2]*Institutes for Robotics and Intelligent Manufacturing, Chinese Academy of Sciences, Shenyang 110016, China*
[3]*University of Chinese Academy of Sciences, Beijing 100049, China*
[4]*Hangzhou Innovation Institute, Beihang University, Hangzhou 310051, China*

Correspondence should be addressed to Bi Zhang; zhangbi@sia.cn and Xingang Zhao; zhaoxingang@sia.cn

Received 26 April 2022; Accepted 11 August 2022; Published 14 September 2022

Academic Editor: Chen Pengyun

Copyright © 2022 Feilong Zhang et al. This is an open access article distributed under the Creative Commons Attribution License, which permits unrestricted use, distribution, and reproduction in any medium, provided the original work is properly cited.

Building a simulated weightless test system on the ground while making comprehensive comparisons of design controllers for a large and heavy multijointed space station robot is not an easy task. To save cost and improve the efficiency of the test, this paper develops a plan in which controllers undergo preliminary testing in a 6-DOF industrial robot. The key idea is gravity compensation included within the dynamic control algorithm of the robot to replace the function of the microgravity environment. It is generally difficult to build an accurate dynamic model for a serial-joint robot in a practical manner. Therefore, to guarantee the stability of the 6-DOF industrial robot in which the dynamic model is built inaccurately, we propose one of the simplest variable structure (VS) controllers, and the stability of the system is analyzed through the Lyapunov method. Last, experiments are carried out to provide preliminary comparisons among three potential algorithms for the space robot in a low-cost and efficient approach.

1. Introduction

Space robots have been playing an important role in orbital servicing missions, such as assisting the assembly of space stations, capturing or repairing faulty satellites, and cleaning orbital debris [1–5]. The primary characteristics of applied space equipment controllers are typically simple but reliable and effective. At present, there is a lack of confidence in launching equipment controlled by complex advanced control algorithms into space considering the risk and price of failure. Space-bound robots are used to serve the corresponding space station routines and tasks, after their performance and reliability in various types of working conditions are verified by trial and error, and under the simulated weightlessness or microgravity environment on the ground. Furthermore, without the weightlessness simulation system, the space robot designed for the space station may not even carry its own weight on the ground. To date, a variety of strategies have been published to compensate for the gravity of space robots for experimental tests on the ground. [6] emulates the zero-gravity environment for the space manipulator using an air-bearing platform, while the platform is mainly suitable for the planar mechanism whose motion is parallel to the air-bearing table [7]; A microgravity environment can also be created in a plane while in a free fall or a free-falling capsule at the microgravity center; however, the test time is too short, and available space for the robot is limited [8–10]; A microgravity test can be performed in the pool using neutral buoyancy. Nevertheless, the influence of fluid damping on test results cannot be negligible [11]; [12–15] emulate the process of capturing the space target by the free-floating robot mounted on satellites, using two industrial robots. However, the purpose is not to create the microgravity environment for the space robot but to generate the trajectory of the satellite; [16–19] design the suspension system to provide the zero gravity of the space robot for maintaining tension. However, it is difficult to remove the influences of the test results caused by the coupled vibration of the serial multijoint space robot and suspension system. Unfortunately, building a simulated weightless test system

for a large and heavy serial multijoint space station robot while choosing the most practical control algorithm from potential candidates is not a simple task and consumes a large amount of time, manpower, auxiliary facilities, and material resources [6–21].

The central difference between the controller designed for a space robot and that for an industrial robot on the ground is determined by considering gravity compensation or not. The gravity compensation included in the dynamic control algorithm of industrial robots can be regarded as a replacement for simulated weightless system functions. As a result, preliminary comparisons between various potential dynamic control algorithms on a 6-DOF industrial robot can be made to save cost and improve the efficiency of the test. This allows contrasting effects to be obvious and easily acquired, which provides prior knowledge and makes preliminary judgment regarding controllers designed for the space robot.

To achieve high precision and efficiency of robot tracking performance, it is necessary to introduce the robotic dynamics into the controller to reduce the effect of robotic nonlinear dynamic characteristics. The dynamics of serial-link robots have been well covered by almost all standard robotic textbooks [22–27]. Two main approaches are feedforward control and computed torque control [28], and both are based on robotic dynamics combined with one diagonal PD controller. Compared with computed torque control, the feedforward control is computationally less expensive at operating time and more easily realizes a high servo rate. This is all possible because the model-based dynamic compensation is "outside" the servo loop, and then, a fast inner servo loop is achieved. Furthermore, PD plus dynamic feedforward compensation in [22] is one of the simplest and most appealing dynamic controllers for robots [29]. It consists of one linear PD feedback and a nominal robot dynamic model computed as a function along the desired path only. Therefore, the advantage of the simple and efficient structure of this type of algorithm provides a reference to the controller design of the space robot.

Generally, the motion control of robots is not an easy task due to nonlinearity, strong coupling, uncertain modeling structure, or parameters. These factors may cause inaccurate joint motion and lead to poor robot performance. To solve these problems, various dynamic feedforward compensation plus PID-like or plus other single-loop feedback control algorithms and computed torque control-based methods have been proposed, including sliding-mode control (SMC) [30–36] or some other variable structure controllers [37–40], neural networks [41–46], fuzzy control [47, 48], and adaptive control [49, 50]. However, many of them are only tested in simulations or double-jointed robotic systems and may have more difficulties achieving the expected performance in the multijoint serial robotic system. One reason is that the current advanced control algorithms, such as neural networks, fuzzy control, and adaptive control, are characterized by complex structures and are time-consuming, and their computational time is possibly several times larger than the commercial robot servo period which is generally less than 10 ms. This may lead to poor real-time performance, let alone the current situation that most of those advanced control algorithms are mainly based on the computed torque control structure. Furthermore, reliable and practical controllers are always those simple ones in experience. At present, there is a lack of confidence to launch space robots controlled by those complex advanced control algorithms into space on account of the risk and price of failure. By comparison, a kind of variable structure controller is proposed in this paper to enhance the tracking performance of the robot under modeling uncertainty. It shows higher efficiency and a better control performance than [22] in the experiment because it combines the PD plus dynamic feedforward compensation and the Bang-Bang control to achieve compensation for the tracking error caused by the modeling uncertainty. One noticeable merit of the proposed method lies in the easier design and application in real robot systems than the controllers designed in [30–48] because of its simplicity in structure.

The main contributions of this paper are summarized as follows: (i) Since testing the different controllers and comparing them in a serial multijoint space station robot on the ground are difficult, this paper initially develops a strategy for controllers to be preliminarily tested in an industrial robot. The key idea is the gravity compensation included in the dynamic control algorithm of the robot to act in the function of a microgravity environment. It will be more efficient to obtain the superior controller from others; (ii) [22] points out that the dynamic model is always known to be inaccurate, and one reason is that it is severely challenging to acquire the structure of the friction model, let alone the corresponding parameters. To improve the control performance of the system, we propose the simplest variable structure control through the combination of the PD plus dynamic feedforward compensation and the Bang-Bang control together to compensate for tracking error caused by the modeling uncertainty, and the stability of the system is analyzed by Lyapunov theory. Then, we experiment to provide preliminary comparisons among several potential algorithms for the space robot in a low-cost and highly efficient way.

The rest of the paper is organized as follows. In Section 2, the dynamic parameters of the robot are identified by the least square method. In Section 3, to guarantee the stability of the system under the modeling uncertainty, a variable structure controller is designed based on the Lyapunov direct method. Then, we design the PD plus and the cascaded PD plus dynamic feedforward compensation to make an experimental comparison in Section 4. As a result, the cascaded PD plus dynamic feedforward compensation control more easily achieves the high-precision tracking performance than the proposed VS control or the PD plus, under the roughly built robotic dynamics. Finally, we present the conclusions in Section 5.

2. Identification of Dynamic Parameters

A typical 6-DOF serial industrial robot is shown in Figure 1.

Figure 1: 6-DOF serial robot.

The dynamic equation of the 6-link robot is written as

$$\tau = M(q)\ddot{q} + C(q,\dot{q})\dot{q} + G(q) + f_c \operatorname{sign}(\dot{q}) + f_v\dot{q}, \quad (1)$$

where $q \in R^{6\times1}$ is the vector of joint displacements, $\tau \in R^{6\times1}$ is the vector of applied torque, $M(q) \in R^{6\times6}$ is the mass matrix of the manipulator, $C(q,\dot{q}) \in R^{6\times6}$ is the centrifugal/Coriolis force matrix, $G(q) \in R^{6\times1}$ is the vector of gravity terms, and $f_v \in R^{6\times6}$ and $f_c \in R^{6\times6}$ are diagonal matrices that consist of the viscous and Coulomb friction parameters, respectively.

Then, in accordance with [51], (1) can be rewritten into the following linear form with $n \times N_s = 6 \times 13$ identifiable base parameters:

$$\tau = Y(q,\dot{q},\ddot{q})p, \quad (2)$$

where

$$p_{78\times1} = [p_1,\cdots,p_6]^T,$$
$$p_i = \left[m_i, mx_i, my_i, mz_i, I_{ai}, I_{xxi}, I_{xyi}, I_{xzi}, I_{yyi}, I_{yzi}, I_{zzi}, f_{ci}, f_{vi}\right]^T. \quad (3)$$

Obviously, 6×13 unknown parameters constitute the dynamic parameters (3) of the robot. We generally reformulate (2) on account that not all parameters in p are independent. In this paper, the independent parameters are collected through QR decomposition.

We perform the robot under a random trajectory to obtain the multiple matrices $Y(\cdot)$ which form the matrix

$$[W]_{6M\times78} = \begin{bmatrix} Y(q(t_1),\dot{q}(t_1),\ddot{q}(t_1)) \\ \vdots \\ Y(q(t_M),\dot{q}(t_M),\ddot{q}(t_M)) \end{bmatrix}. \quad (4)$$

The number of matrices $Y(\cdot)$ or the sample number is $M = 10000$. The sample period is 0.1 s. We apply QR decomposition (5) to find the independent base dynamic parameters, with the orthonormal matrix $Q \in \mathbb{R}^{Mn\times nNs}$ and upper triangular matrix R:

$$W = QR. \quad (5)$$

Supposing that the main diagonal elements r_{ll} in the lth column of R are zero, the corresponding columns of R are collected in R_2, while the rest constitute R_1:

$$R = [R_1\ R_2]. \quad (6)$$

Similarly, the corresponding columns of W are collected consistent with R. According to (2), we have

$$W\pi = \left[[W_1]_{6M\times52}\ [W_2]_{6M\times26}\right]\begin{bmatrix}\pi_1 \\ \pi_2\end{bmatrix} = T = \begin{bmatrix}\tau(1) \\ \vdots \\ \tau(M)\end{bmatrix}, \quad (7)$$

with independent π_1 and dependent π_2 which are collected from p in the same way as W.

According to (6) and (7), we have

$$T = W_1\pi^* \triangleq W_1(\pi_1 + k\pi_2), \quad (8)$$

where $k = R_2R_1^{-1}$.

Then, the unknown dynamic parameters are estimated by

$$[\pi^*]_{52\times1} = \left(W_1{}^T W_1\right)^{-1} W_1{}^T T. \quad (9)$$

The excitation reference trajectories for every joint are applied with the finite sum of 5 harmonic sine and cosine functions. The joint position, velocity, and acceleration of the ith joint are

$$q_i(t) = \sum_{l=1}^{5}\left[\frac{a_l}{w_f l}\sin\left(w_f lt\right) - \frac{b_l}{w_f l}\cos\left(w_f lt\right) + q_{i0}\right],$$
$$\dot{q}_i(t) = \sum_{l=1}^{5}\left[a_l\cos\left(w_f lt\right) + b_l\sin\left(w_f lt\right)\right],$$
$$\ddot{q}_i(t) = w_f\sum_{l=1}^{5}\left[a_l l\cos\left(w_f lt\right) + b_l l\sin\left(w_f lt\right)\right], \quad (10)$$

where the fundamental frequency is $w_f = 0.05$ and q_{i0} is the offset of the joint position of the trajectory. The parameters a_l and b_l are determined by trial and error or the following optimization process. The excitation trajectory $q^*(t)$ is determined by the optimization issue of (11) which is directly equivalent to optimizing the condition number for less estimation error while having less complexity and

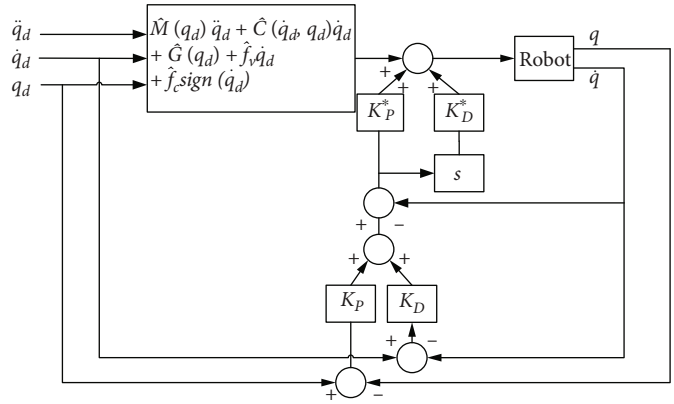

Figure 2: Control scheme of the robot.

Table 1: Controller parameters of each joint.

Joint	K_P ; K_D	r_i
1	962260; 80000	1000
2	886260; 209500	100
3	209500; 69000	100
4	1852500; 42000	1000
5	489500; 26700	1000
6	87000; 7500	7000

calculation time:

$$q^*(t) = \arg\min(W_1) \tag{11}$$

subject to

$$-q_{\max\, i} \le q_i(t) = \sum_{l=1}^{5} \frac{a_l}{w_f l} \sin\left(w_f l t\right) - \frac{b_l}{w_f l} \cos\left(w_f l t\right) \le q_{\max\, i}, \tag{12}$$

$$-v_{\max\, i} \le \dot{q}_i(t) = \sum_{l=1}^{5} a_l \cos\left(w_f l t\right) + b_l \sin\left(w_f l t\right) \le v_{\max\, i}, \tag{13}$$

$$-a_{\max\, i} \le \ddot{q}_i(t) = w_f \sum_{l=1}^{5} a_l l \cos\left(w_f l t\right) + b_l l \sin\left(w_f l t\right) \le a_{\max\, i}, \tag{14}$$

$$q_i(t_0) = q_i(0) = \sum_{i=1}^{5} \frac{b_l}{w_f l} + q_{i0} = 0, \tag{15}$$

$$\dot{q}_i(t_0) = \dot{q}_i(0) = \sum_{i=1}^{5} a_l = 0, \tag{16}$$

$$\ddot{q}_i(t_0) = \ddot{q}_i(0) = \sum_{i=1}^{5} w_f l b_l = 0, \tag{17}$$

where $q_{\max} = [q_{\max\,1}, \cdots, q_{\max\,6}]^T = [153, 24, 40, 153, 90, 180]^T /180\pi$, $v_{\max} = [v_{\max\,1}, \cdots, v_{\max\,6}]^T = [296, 240, 310, 355, 267, 500]^T/180\pi$, and $a_{\max} = [a_{\max\,1}, \cdots, a_{\max\,6}]^T = [1800, 1500, 1800, 1800, 1300, 3000]^T/180\pi$ are the constraint vectors for position, velocity, and acceleration, respectively.

It is possible to use any optimization method to solve the above optimization problem. In this paper, the parameters a_l and b_l are solved by the interior-point method. The maximum number of iterations is 20000. The initial values of a_l and b_l are chosen as random numbers within $[-0.5, 0.5]$.

The dynamic model is often not known accurately. For example, the structure of the friction model is generally difficult to know, let alone the parameter values. Furthermore, it is unrealistic to have precise parameter values in the model at all times through applying the least square method [51, 52] in one time since the dynamic parameters always change as the robot moves. Therefore, the following controller is inevitably designed in accordance with the inaccurate dynamic parameters.

3. Controller Design

The robotic dynamic model has the following properties [23, 27]:

(P1)The matrix $M(q)$ is positive definite symmetric and satisfies $\underline{M}\|x\|^2 \le x^T M(q) x \le \bar{M}\|x\|^2$ for positive constants $\bar{M}$, $\underline{M} > 0$

(P2)$\dot{M}(q) - 2C(q, \dot{q})$ is skew-symmetric

(P3)The matrix $C(q, \dot{q})$ satisfies $\|C(q, \dot{q})\| \le \mu_c$ for positive constant $\mu_c > 0$

(P4) The vector $G(q)$ satisfies $\|G(q)\| \le \mu_g$ for positive constant $\mu_g > 0$

From (9), we can obtain $\widehat{M}(q)$, $\widehat{C}(q, \dot{q})$, $\widehat{G}(q)$, $\widehat{f}_c$, and $\widehat{f}_v$ which represent the estimation of $M(q)$, $C(q, \dot{q})$, $G(q)$, f_c, and f_v, respectively. Define $\tilde{M}(q) = \widehat{M}(q_d) - M(q)$, $\tilde{C}(q, \dot{q}) = \widehat{C}(q_d, \dot{q}_d) - C(q, \dot{q})$, $\tilde{G}(q) = G(q_d) - G(q)$, and the nonnegative definite diagonal gain matrices K_P, K_D, and $\Upsilon = \text{diag}(r_1, \cdots, r_6)$; $q_d = [q_1^*, \cdots, q_6^*]^T$ represents the desired trajectory for the robot joints.

Table 2: Estimated dynamic parameters of the robot.

Parameters	Joint 1	Joint 2	Joint 3	Joint 4	Joint 5	Joint 6
m_i (kg)	10	10	10	10	10	10
mx_i (kg·m)	0.000000	1467.621893	120.973665	0.877570	-5.497015	-3.474394
my_i (kg·m)	0.000000	-485.168899	512.922191	-4.105343	49.201786	9.947225
mz_i (kg·m)	0.000000	0.000000	0.000000	0.000000	0.000000	0.000000
I_{xxi} (kg·m^2)	0.000000	-3105.984543	-429.633816	139.535980	-35.190459	-5.898670
I_{xyi} (kg·m^2)	0.000000	-2279.068182	175.632270	-37.783294	-5.612843	4.712513
I_{xzi} (kg·m^2)	0.000000	-168.579890	137.144088	1.357674	-25.300536	-3.631684
I_{yyi} (kg·m^2)	0.000000	-2153.914022	-14.634628	-0.000770	-0.030217	-0.012071
I_{yzi} (kg·m^2)	0.000000	-467.555176	158.191065	-34.563860	-15.506560	-19.074189
I_{zzi} (kg·m^2)	1355.845148	-4625.319065	315.581754	123.918230	39.386756	-10.111644
I_{ai} (kg·m^2)	0.000000	0.000000	-1198.010476	81.708986	-14.478101	-27.911115
f_{ci} (Nm·s/rad)	5469.258178	4450.476442	8730.326694	2888.554652	1857.202169	-2029.910574
f_{vi} (Nm·s/rad)	7102.364470	31212.701099	16441.785926	3909.460084	1322.947888	1322.947888

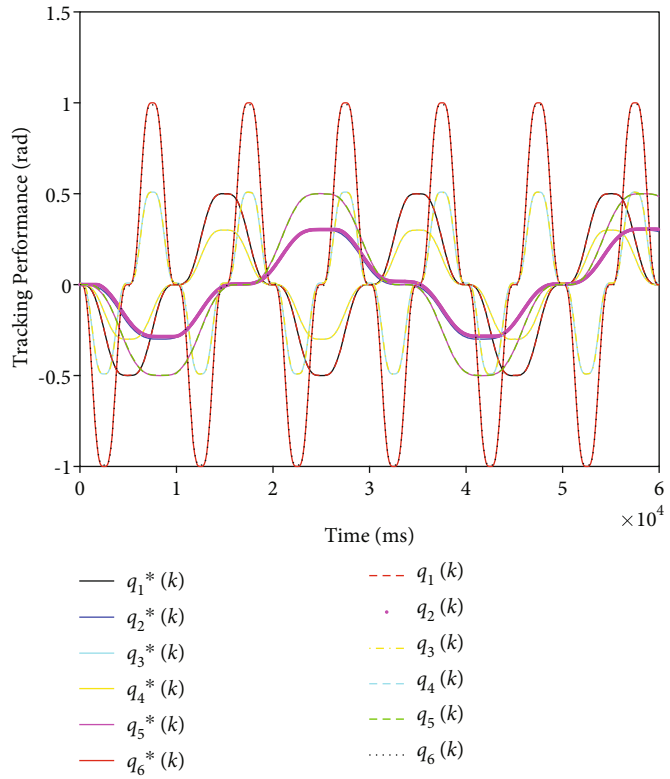

Figure 3: Tracking performance of each robotic joint controlled by variable structure control.

Define $e = q_d - q$. We choose the Lyapunov function

$$V = \frac{1}{2}\dot{e}^T M(q)\dot{e} + \frac{1}{2}e^T K_P e, \tag{18}$$

which is continuous and nonnegative. According to the properties of the robotic dynamic model, we can obtain (19) by differentiating (18) as follows:

$$\begin{aligned}\dot{V} &= \dot{e}^T M(q)\ddot{e} + \frac{1}{2}\dot{e}^T \dot{M}(q)\dot{e} + \dot{e}^T K_P e \\ &= \dot{e}^T (M(q)\ddot{e} + C(q,\dot{q})\dot{e} + K_P e) \\ &= \dot{e}^T (M(q)\ddot{q}_d + C(q,\dot{q})\dot{q}_d + K_P e \\ &\quad + G(q) + f_c \operatorname{sign}(\dot{q}) + f_v \dot{q} - \tau).\end{aligned} \tag{19}$$

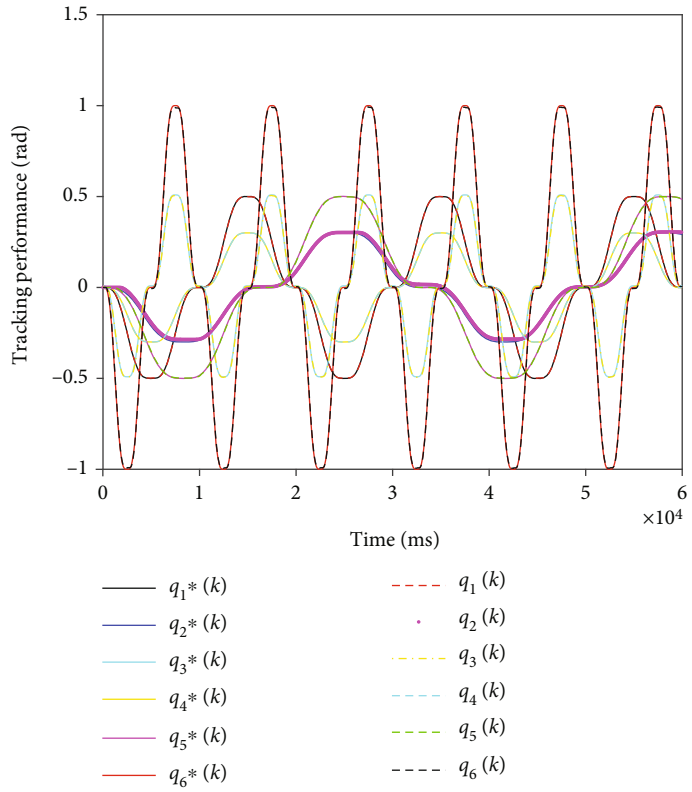

Figure 4: Tracking performance of each robotic joint controlled by PD plus.

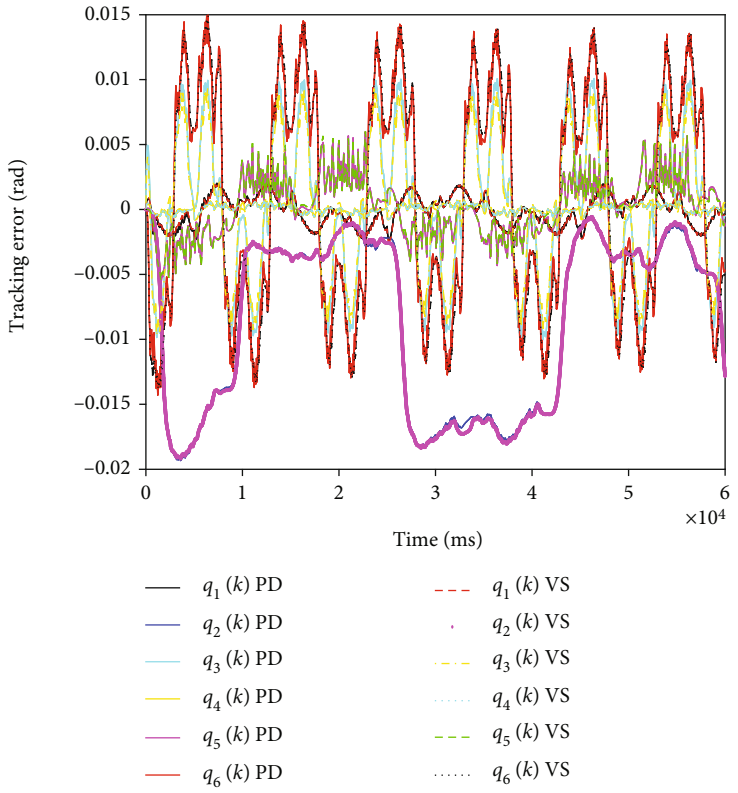

Figure 5: Tracking error comparison between variable structure control and PD plus.

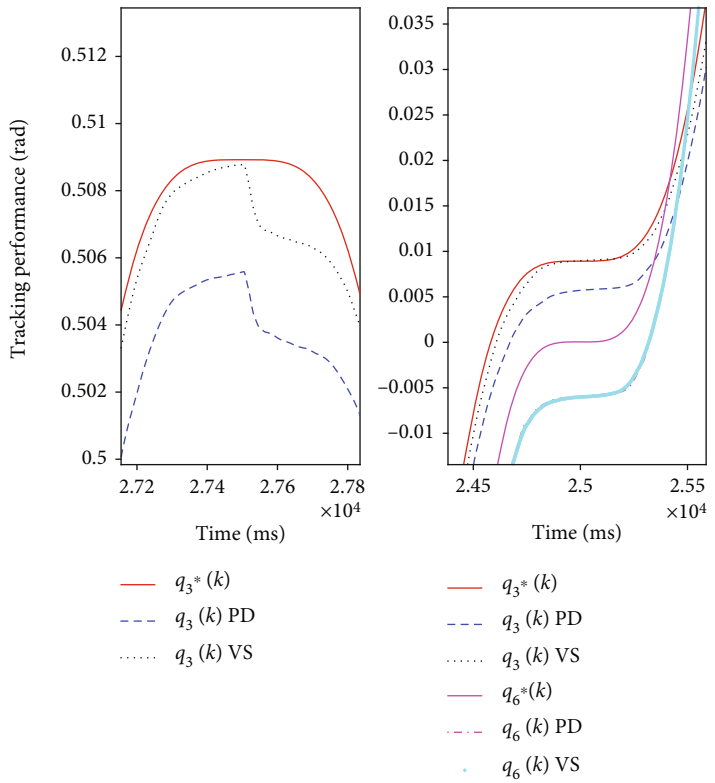

Figure 6: Tracking performance of the 3rd joint and the 6th joint of the robot controlled by variable structure control and PD plus.

Table 3: Controller parameters of each joint.

Joint	$K_P; K_D$	$K_P^*; K_D^*$
1	800; 0.1	800; 70
2	650; 0.1	6000; 15
3	1000; 0.1	2500; 60
4	650; 0.1	250; 40
5	800; 0	600; 15
6	650; 0.1	600; 15

Then, we design the controller

$$\tau = \tau_{\text{dynamic}} + \tau_{\text{PD}}, \tag{20}$$

$$\begin{aligned}\tau_{\text{dynamic}} = {} & \hat{M}(q_d)\ddot{q}_d + \hat{C}(q_d, \dot{q}_d)\dot{q}_d + \hat{G}(q_d) \\ & + \hat{f}_c \text{ sign } (\dot{q}_d) + \hat{f}_v \dot{q}_d,\end{aligned} \tag{21}$$

$$\tau_{\text{PD}} = K_P e + K_D \dot{e} + \Upsilon \text{ sign } (\dot{e}) \tag{22}$$

to have

$$\begin{aligned}\dot{V} &= -\dot{e}^T (K_D \dot{e} + \bar{\sigma} + \Upsilon \text{ sign } (\dot{e})) \\ &= -\dot{e}^T K_D \dot{e} - \dot{e}^T \bar{\sigma} - \dot{e}^T \Upsilon \text{ sign } (\dot{e}),\end{aligned} \tag{23}$$

where

$$\begin{aligned}\bar{\sigma} &= \tilde{M}(q)\ddot{q}_d + \tilde{C}(q, \dot{q})\dot{q}_d + \tilde{G}(q) + \tilde{F}_f, \\ \tilde{F}_f &= \hat{f}_c \text{ sign } (\dot{q}_d) - f_c \text{ sign } (\dot{q}) + \hat{f}_v \dot{q}_d - f_v \dot{q}.\end{aligned} \tag{24}$$

Herein, we choose

$$r_i > \|\bar{\sigma}\|_{\max}, \tag{25}$$

to have

$$\dot{V} < 0. \tag{26}$$

For the case $n = 6$, the iterative Newton-Euler scheme is approximately 100 times more efficient than the Lagrangian approach. Consequently, we normally realize (21) by the iterative Newton-Euler dynamics shown as follows.

(a) Outward Iterations $i : 0 \longrightarrow 5$

The joint $i + 1$ rotational velocity is

$$w_{i+1} = R_i^{i+1} w_i + \dot{q}_{i+1}^* \hat{Z}_{i+1}, \tag{27}$$

where $\hat{Z}_{i+1}$ represents the axis pointing along the $i + 1$th joint axis and R_i^{i+1} is the rotation matrix.

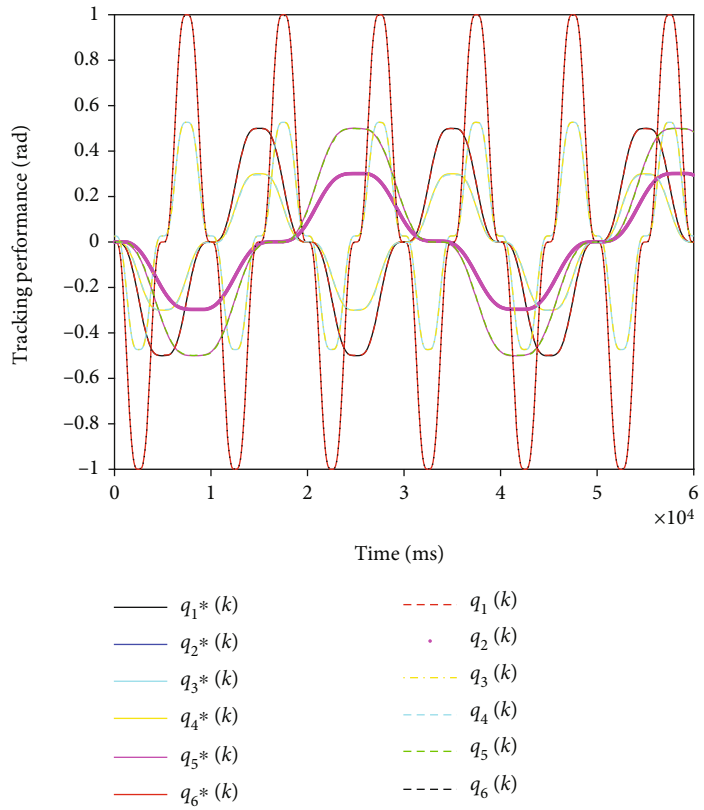

Figure 7: Tracking performance of each robotic joint controlled by cascaded PD plus.

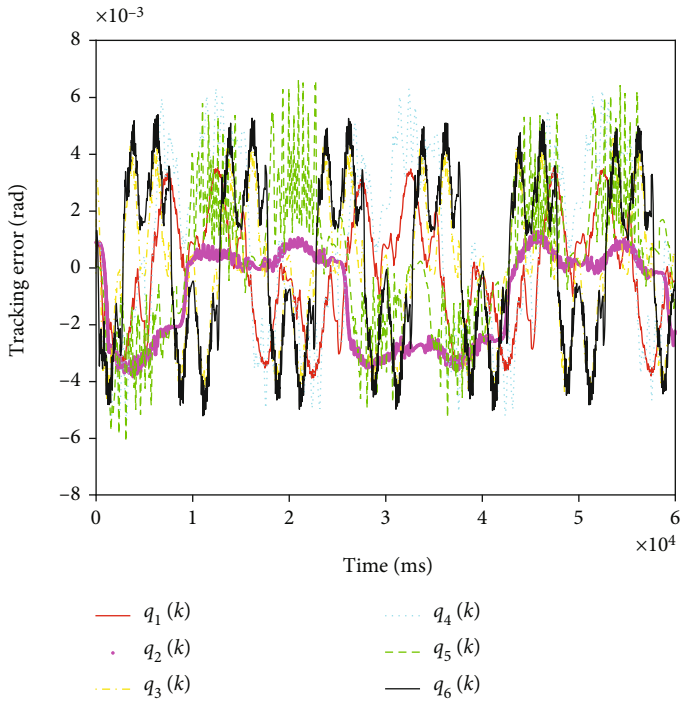

Figure 8: Tracking error of each robotic joint controlled by cascaded PD plus.

The angular acceleration from one link to the next is described by

$$\dot{w}_{i+1} = R_i^{i+1}\dot{w}_i + R_i^{i+1}w_i \times \dot{q}_{i+1}\widehat{Z}_{i+1} + \ddot{q}_{i+1}^{*}\widehat{Z}_{i+1}. \quad (28)$$

Noticeably, (27) and (28) are different from the iterations in the textbook [22], since the velocity in (27) and acceleration in (28) of each joint are the desired velocity and acceleration, respectively.

Then, we obtain the linear acceleration of each link-frame origin through

$$\dot{v}_{i+1} = R_i^{i+1}\left(\dot{w}_i \times P_i^{i+1} + w_i \times \left(w_i \times P_i^{i+1}\right) + \dot{v}_i\right) \quad (29)$$

and obtain the linear acceleration of the center of mass of each link

$$\dot{v}_{C_{i+1}}^{i+1} = \dot{w}_{i+1} \times P_{C_{i+1}}^{i+1} + w_{i+1} \times \left(w_{i+1} \times P_{C_{i+1}}^{i+1}\right) + \dot{v}_{i+1}, \quad (30)$$

where $\{C_i\}$ represents a frame attached to each link and has its origin located at the center of mass of the link with the same orientation as the link frame $\{i\}$; $P_{C_{i+1}}^{i+1}$ locates the position of $\{C_{i+1}\}$ relative to the $i+1$th joint.

Then, we can obtain the inertial force and torque acting at the center of the mass of each link (31) and (32) through Newton-Euler equations as follows:

$$F_{i+1} = m_{i+1}\dot{v}_{i+1}^{C_{i+1}}, \quad (31)$$

$$N_{i+1} = I_{i+1}^{C_{i+1}}\dot{w}_{i+1} + w_{i+1} \times I_{i+1}^{C_{i+1}}w_{i+1}, \quad (32)$$

where $I_{i+1}^{C_{i+1}}$ determines the mass moments of inertia relative to the center of mass in the $i+1$th link.

(b) Inward Iterations $i : 6 \longrightarrow 1$

The force exerted on link i by link $i-1$ is

$$f_i = R_{i+1}^{i}f_{i+1} + F_i. \quad (33)$$

12The torque exerted on link i by link $i-1$ is

$$n_i = N_i + R_{i+1}^{i}n_{i+1} + P_{C_i}^{i} \times F_i + P_{i+1}^{i} \times R_{i+1}^{i}f_{i+1}. \quad (34)$$

Finally, we obtain the required joint torques

$$\tau_i = n_i^T\widehat{Z}_i, \quad (35)$$

which constitute $\tau_{\text{dynamic}} = [\tau_1, \cdots, \tau_6]^T$ in (21).

Controller (20) guarantees the stability of the system in theory. Furthermore, if we let $r_i = 0, i = 1, \cdots, 6$, the controller is the feedforward nonlinear control shown in Figure 10.6 in [22]. Furthermore, if we correct τ_{PD} (22) into the following cascaded PD controller

$$\tau_{\text{PD}} = K_P^{*}[(K_P e + K_D\dot{e}) - \dot{q}] + K_D^{*}\frac{d}{dt}[(K_P e + K_D\dot{e}) - \dot{q}], \quad (36)$$

which uses PD in both the outer loop and inner loop, and then, the cascaded PD plus dynamic feedforward control is shown in Figure 2.

The position control loop (outer loop) is to maintain the positional trajectory tracking. The error in the position control loop provides the desired velocity for the velocity loop (inner loop). We apply a PD controller $(K_P e + K_D\dot{e})$ on the basis of the error between the desired and actual positions to generate the desired speed of the motor so that the actual position tracks the desired position closely. The velocity loop uses the PD controller plus dynamic feedforward compensation to generate the desired torque for the robot joint (motor) so that the actual velocity tracks the desired velocity closely. We normally adjust the gains of the joint controller: K_P, K_D, K_P^{*}, and K_D^{*} to change the behaviors of the robot subject to variation in the dynamic model caused by various poses and payloads, variation in friction with temperature and time, and some disturbance torques owing to complicated velocity and acceleration coupling.

By removing the gravity compensation item of the controller (20), we can obtain the practical controller for the on-orbit space robot:

$$\tau = \widehat{M}(q_d)\ddot{q}_d + \widehat{C}(q_d, \dot{q}_d)\dot{q}_d + \widehat{f}_c \text{ sign } (\dot{q}_d) + \widehat{f}_v\dot{q}_d + \tau_{\text{PD}}. \quad (37)$$

4. Experiment

The proposed variable structure method is applied to the robot, and the controller parameters of each joint are listed in Table 1. The estimated dynamic parameters of the robot are shown in Table 2. The tracking performance of each robotic joint is shown in Figure 3.

When we let $r_i = 0\,(i = 0, \cdots, 6)$, the proposed variable structure controller degenerates into the PD plus. The tracking performance of each robotic joint controlled by PD plus is shown in Figure 4. The tracking error comparison between VS control and PD plus is shown in Figure 5.

Figures 3 and 4 show that both outputs of the robot controlled by the proposed VS control and PD plus are able to track the desired trajectories. Figure 5 shows that the tracking error curves of the robot controlled by the proposed VS method and PD plus are close. Hence, the drawing of partial enlargement of the output of the 3rd joint and the output of the 6th joint of the robot controlled by variable structure control and PD plus are shown in Figure 6 to make a further comparison.

Figure 6 shows that the tracking performance of the 3rd joint of the robot controlled by the proposed VS control is better than that controlled by PD plus for less tracking error from 27200 ms to 27800 ms and from 24500 ms to 25500 ms, while there is no obvious difference between the two methods acting at the 6th joint. These findings are possibly because the proposed VS control combines the PD plus dynamic feedforward compensation and the Bang-Bang control together, and the Bang-Bang control item Υ sign $(\dot{e}$) can be used to suppress all matching uncertainties and unpredictable system dynamics. In this experiment, the

Bang-Bang control item can provide timely compensation for more tracking errors caused by the modeling uncertainty and consequently improves both the tracking accuracy and tracking speed of the robot.

Then, we apply cascaded PD plus dynamic feedforward compensation control to the robotic manipulator for comparison with the aforementioned two methods. The cascaded PD controller parameters of each joint are listed in Table 3.

The tracking performance of each robotic joint is shown in Figure 7. The tracking error of each joint controlled by cascaded PD plus is shown in Figure 8.

With less effort spent on the adjustment of controller parameters in the experiment, the cascaded PD plus easily guarantees the tracking error of each joint of the robot within $\pm 8 \times 10^{-3}$ rad which is shown in Figure 8. The reason is summarized as follows: As demanded by the outer loop, the inner loop is adopted to generate the desired torque for the robot joint so that the actual velocity tracks the desired velocity closely. The outer loop is used to determine the velocity of the joint that minimizes position error. By comparison, we have tested the proposed VS control and PD plus by trial and error in our experiment to guarantee the tracking error of each joint of the robot within $\pm 2 \times 10^{-2}$ rad which is shown in Figure 5. By comparing Figures 8 and 5, we find that the cascaded PD plus dynamic feedforward compensation control more easily guarantees the high-precision tracking performance than the proposed VS control or the PD plus in the experiment, under the roughly built robotic dynamics. Actually, the PD plus typically represents a class of single-loop feedback control. Furthermore, this also implies that many SMC or other variable structure controls based on a single-loop feedback strategy may not more easily achieve better performance than the cascaded PD method. Based on this, we recommend the cascaded PID plus feedforward dynamic model for the calculation of the desired torque in the 6-DOF serial robot rather than the single-loop feedback strategy. The controller structure may be more important than the adjustment of the controller parameters in the robotic system.

The controller design or the choice of the controller from different candidates for the space robot remains prudent work. One purpose of the above analyses and experimental results is to provide a source of prior knowledge and practice experience for the controller design and the test of the space robot. Furthermore, by removing gravity compensation, we can design the controller of the space station robot in the same way as the above controllers of the industrial robot.

5. Conclusions

To suggest simple yet effective controllers for the large and heavy serial multijoint space station robot, we made comparisons among our proposed variable structure method, PD plus and the cascaded PD plus on the industrial robot in this paper. First, the dynamic parameters of the robot are identified by the least square method. Second, to guarantee the stability of the system under modeling uncertainty in theory, a variable structure controller is designed based on the Lyapunov direct method. It can be separated into two parts: the PD plus and the sign function. Third, experiments show that the cascaded PD plus dynamic feedforward compensation control more easily guarantees the high-precision tracking performance than the proposed variable structure control or the PD plus, under the roughly built robotic dynamics.

Data Availability

The experimental data used to support the findings in this paper can be available from the first author and corresponding author upon request.

Conflicts of Interest

The authors declare that they have no conflicts of interest.

Acknowledgments

This work is supported by the National Natural Science Foundation of China under Grant Number 62103406 and is also supported by the Natural Science Foundation of Liaoning Province under Grant Number 2021-MS-032.

References

[1] X. Zhang, J. Liu, J. Feng, Y. Liu, and Z. Ju, "Effective capture of nongraspable objects for space robots using geometric cage pairs," *IEEE/ASME Transactions on Mechatronics*, vol. 25, no. 1, pp. 95–107, 2020.

[2] X. Zhang and J. Liu, "Effective motion planning strategy for space robot capturing targets under consideration of the berth position," *Acta Astronautica*, vol. 148, pp. 403–416, 2018.

[3] P. Huang, L. Chen, B. Zhang, Z. Meng, and Z. Liu, "Autonomous rendezvous and docking with nonfull field of view for tethered space robot," *International Journal of Aerospace Engineering*, vol. 2017, Article ID 3162349, 11 pages, 2017.

[4] Y. Wang, X. Liang, K. Gong, and Y. Liao, "Kinematical research of free-floating space-robot system at position level based on screw theory," *International Journal of Aerospace Engineering*, vol. 2019, Article ID 6857106, 13 pages, 2019.

[5] S. Sun, C. Wei, Z. Huang et al., "Adaptive control of space robot despinning tumbling target using flexible brushes," *International Journal of Aerospace Engineering*, vol. 2021, Article ID 6196556, 9 pages, 2021.

[6] M. Sabatini, P. Gasbarri, and G. B. Palmerini, "Coordinated control of a space manipulator tested by means of an air bearing free floating platform," *Acta Astronautica*, vol. 139, pp. 296–305, 2017.

[7] Z. Chen, Z. Luo, Y. Wu, W. Xue, and W. Li, "Research on high-precision attitude control of joint actuator of three-axis air-bearing test bed," *Journal of Control Science and Engineering*, vol. 2021, Article ID 5582541, 11 pages, 2021.

[8] Y. Watanabe and Y. Nakamura, "Experiments of a space robot in the free-fall environment," *Artificial Intelligence, Robotics and Automation in Space*, vol. 440, article 601, 1999.

[9] C. Menon, A. Aboudan, S. Cocuzza, A. Bulgarelli, and F. Angrilli, "Free-flying robot tested on parabolic flights:

kinematic control," *Journal of Guidance, Control, and Dynamics*, vol. 28, no. 4, pp. 623–630, 2005.

[10] C. Menon, S. Busolo, S. Cocuzza et al., "Issues and solutions for testing free-flying robots," *Acta Astronautica*, vol. 60, no. 12, pp. 957–965, 2007.

[11] Y. Yuan, P. Zhang, Z. Wang, L. Guo, and H. Yang, "Active disturbance rejection control for the ranger neutral buoyancy vehicle: a delta operator approach," *IEEE Transactions on Industrial Electronics*, vol. 64, no. 12, pp. 9410–9420, 2017.

[12] I. Rekleitis, E. Martin, G. Rouleau, R. L'Archevêque, K. Parsa, and E. Dupuis, "Autonomous capture of a tumbling satellite," *Journal of Field Robotics*, vol. 24, no. 4, pp. 275–296, 2007.

[13] F. Aghili, "A prediction and motion-planning scheme for visually guided robotic capturing of free-floating tumbling objects with uncertain dynamics," *IEEE Transactions on Robotics*, vol. 28, no. 3, pp. 634–649, 2012.

[14] H. Liu, B. Liang, W. Xu, D. Zhang, and X. Wang, "A ground experiment system of a free-floating robot for fine manipulation," *International Journal of Advanced Robotic Systems*, vol. 9, no. 5, p. 183, 2012.

[15] R. Lampariello, H. Mishra, N. Oumer, P. Schmidt, M. de Stefano, and A. Albu-Schaffer, "Tracking control for the grasping of a tumbling satellite with a free-floating robot," *IEEE Robotics and Automation Letters*, vol. 3, no. 4, pp. 3638–3645, 2018.

[16] H. Fujii, K. Uchiyama, H. Yoneoka, and T. Maruyama, "Ground-based simulation of space manipulators using test bed with suspension system," *Journal of Guidance, Control, and Dynamics*, vol. 19, no. 5, pp. 985–991, 1996.

[17] H. Shi, S. Ma, M. Huo, and N. Qi, "Design and control of a position servo system in the zero gravity simulation of space manipulators," in *2015 International Conference on Fluid Power and Mechatronics (FPM)*, pp. 501–504, Harbin, China, August 2015.

[18] H. B. Brown and J. M. Dolan, "A novel gravity compensation system for space robots," 1994.

[19] Y. He, F. Zhang, M. Yang, and Z. J. J. R. Xu, "Design of tracking suspension gravity compensation system for satellite antenna deployable manipulator," *Robot*, vol. 40, no. 3, pp. 377–384, 2018.

[20] Z. Xu, X. Bai, J. Wang, M. Liu, and X. Zhang, "The control method of force loading of robot on load transfer mechanism of space station," in *2019 IEEE 15th International Conference on Control and Automation (ICCA)*, pp. 518–523, Edinburgh, UK, July 2018.

[21] Y. He, F. L. Zhang, M. Y. Liu, and Z. Xu, "Controller design and accuracy evaluations for the space station sun directional device test system," *Journal of Astronautics*, vol. 39, no. 6, pp. 674–682, 2018.

[22] J. J. Craig, *Introduction to Robotics: Mechanics and Control*, Prentice Hall, Boston, USA, 2004.

[23] M. W. Spong, S. Hutchinson, and M. Vidyasagar, *Robot Modeling and Control*, Wiley, NJ, USA, 2005.

[24] R. P. Paul, "Robot manipulators: mathematics, programming, and control: the computer control of robot manipulators," 1981.

[25] P. I. Corke and O. Khatib, *Robotics, Vision and Control: Fundamental Algorithms in MATLAB*, Springer, Berlin, 2017.

[26] B. Siciliano, O. Khatib, and T. Kröger, *Springer Handbook of Robotics*, Springer, Berlin, 2007.

[27] B. Siciliano, L. Sciavicco, L. Villani, and G. Oriolo, *Robotics: Modelling, Planning and Control*, Springer Science & Business, Berlin, 2010.

[28] S. Moberg and S. Hanssen, "A DAE approach to feedforward control of flexible manipulators," in *Proceedings 2007 IEEE International Conference on Robotics and Automation*, pp. 3439–3444, Rome, Italy, April 2007.

[29] V. Santibañez and R. Kelly, "PD control with feedforward compensation for robot manipulators: analysis and experimentation," *Robotica*, vol. 19, no. 1, pp. 11–19, 2001.

[30] V. Parra-Vega, S. Arimoto, Y. H. Liu, G. Hirzinger, and P. Akella, "Dynamic sliding PID control for tracking of robot manipulators: theory and experiments," *IEEE Transactions on Robotics and Automation*, vol. 19, no. 6, pp. 967–976, 2003.

[31] P. R. Ouyang, J. Acob, and V. Pano, "PD with sliding mode control for trajectory tracking of robotic system," *Robotics and Computer-Integrated Manufacturing*, vol. 30, no. 2, pp. 189–200, 2014.

[32] T. Kara and A. H. Mary, "Adaptive PD-SMC for nonlinear robotic manipulator tracking control," *Studies in Informatics and Control*, vol. 26, no. 1, pp. 49–58, 2017.

[33] S. I. Han and J. Lee, "Finite-time sliding surface constrained control for a robot manipulator with an unknown deadzone and disturbance," *ISA Transactions*, vol. 65, pp. 307–318, 2016.

[34] N. M. H. Norsahperi and K. A. Danapalasingam, "An improved optimal integral sliding mode control for uncertain robotic manipulators with reduced tracking error, chattering, and energy consumption," *Mechanical Systems and Signal Processing*, vol. 142, article 106747, 2020.

[35] X. Zhang, J. G. Liu, Q. Gao, and Z. Ju, "Adaptive robust decoupling control of multi-arm space robots using time-delay estimation technique," *Nonlinear Dynamics*, vol. 100, no. 3, pp. 2449–2467, 2020.

[36] X. Zhang, J. Liu, Y. Tong, Y. Liu, and Z. Ju, "Attitude decoupling control of semifloating space robots using time-delay estimation and supertwisting control," *IEEE Transactions on Aerospace and Electronic Systems*, vol. 57, no. 6, pp. 4280–4295, 2021.

[37] C. Zheng, Y. Su, and P. Mercorelli, "A simple nonlinear PD control for faster and high-precision positioning of servomechanisms with actuator saturation," *Mechanical Systems and Signal Processing*, vol. 121, pp. 215–226, 2019.

[38] Y. Su, C. Zheng, and P. Mercorelli, "Robust approximate fixed-time tracking control for uncertain robot manipulators," *Mechanical Systems and Signal Processing*, vol. 135, article 106379, 2020.

[39] Y. Wang, M. Chen, and Y. Song, "Robust fixed-time inverse dynamic control for uncertain robot manipulator system," *Complexity*, vol. 2021, Article ID 6664750, 12 pages, 2021.

[40] K. Huang, Y. Xian, S. Zhen, and H. Sun, "Robust control design for a planar humanoid robot arm with high strength composite gear and experimental validation," *Mechanical Systems and Signal Processing*, vol. 155, article 107442, 2021.

[41] W. Yu and J. Rosen, "Neural PID control of robot manipulators with application to an upper limb exoskeleton," *IEEE Transactions on cybernetics*, vol. 43, no. 2, pp. 673–684, 2013.

[42] W. He, B. Huang, Y. Dong, Z. Li, and C. Y. Su, "Adaptive neural network control for robotic manipulators with unknown deadzone," *IEEE Transactions on Cybernetics*, vol. 48, no. 9, pp. 2670–2682, 2018.

[43] E. O. Freire, F. G. Rossomando, and C. M. Soria, "Self-tuning of a neuro-adaptive PID controller for a SCARA robot based on neural network," *IEEE Latin America Transactions*, vol. 16, no. 5, pp. 1364–1374, 2018.

[44] D. C. Gandolfo, F. G. Rossomando, C. M. Soria, and R. O. Carelli, "Adaptive neural compensator for robotic systems control," *IEEE Latin America Transactions*, vol. 17, no. 4, pp. 670–676, 2019.

[45] L. A. Soriano, E. Zamora, J. M. Vazquez-Nicolas, G. Hernández, J. A. Barraza Madrigal, and D. Balderas, "PD control compensation based on a cascade neural network applied to a robot manipulator," *Frontiers in Neurorobotics*, vol. 14, 2020.

[46] F. G. Rossomando, E. Serrano, C. M. Soria, and G. Scaglia, "Neural dynamics variations observer designed for robot manipulator control using a novel saturated control technique," *Mathematical Problems in Engineering*, vol. 2020, Article ID 3240210, 14 pages, 2020.

[47] J. Armendariz, V. Parra-Vega, R. García-Rodríguez, and S. Rosales, "Neuro-fuzzy self-tuning of PID control for semiglobal exponential tracking of robot arms," *Applied Soft Computing*, vol. 25, pp. 139–148, 2014.

[48] J. L. Meza, V. Santibáñez, R. Soto, and M. A. Llama, "Fuzzy self-tuning PID semiglobal regulator for robot manipulators," *IEEE Transactions on Industrial Electronics*, vol. 59, no. 6, pp. 2709–2717, 2012.

[49] M. Bagheri, I. Karafyllis, P. Naseradinmousavi, and M. Krstic, "Adaptive control of a two-link robot using batch least-square identifier," *IEEE/CAA Journal of Automatica Sinica*, vol. 8, no. 1, pp. 86–93, 2021.

[50] H. S. Jayakody, L. Shi, J. Katupitiya, and N. Kinkaid, "Robust adaptive coordination controller for a spacecraft equipped with a robotic manipulator," *Journal of Guidance, Control, and Dynamics*, vol. 39, no. 12, pp. 2699–2711, 2016.

[51] J. Jin and N. Gans, "Parameter identification for industrial robots with a fast and robust trajectory design approach," *Robotics and Computer-Integrated Manufacturing*, vol. 31, pp. 21–29, 2015.

[52] M. Neubauer, H. Gattringer, and H. Bremer, "A persistent method for parameter identification of a seven-axes manipulator," *Robotica*, vol. 33, no. 5, pp. 1099–1112, 2015.